Crystallization-Induced Chirality Transfer in Conformationally Flexible Azahelicene Au(I) Complexes with Circularly Polarized Luminescence Activation

Pingyu Jiang,[a]‡ Alexander S. Mikherdov,[b]‡ Hajime Ito,*[a,b] Mingoo Jin*[b]

[a]Division of Applied Chemistry, Graduate School of Engineering, Hokkaido University, Sapporo, Hokkaido 060-8628, Japan

[b]Institute for Chemical Reaction Design and Discovery (WPI-ICReDD), Hokkaido University, Sapporo, Hokkaido, 060-8628, Japan

ABSTRACT: Flexible and twisted annulated π-systems exhibit numerous unique and desirable features owing to their ability to display chirality. However, preventing their racemization due to dynamic nature of their chirality remains a challenge. One promising approach to stabilize homochirality in such systems is chirality transfer from a chiral auxiliary to a moiety displaying dynamic chirality. Herein, we introduce a new approach for dynamic chirality stabilization in conformationally flexible azahelicene species via crystallization-induced intermolecular chirality transfer in Au(I) complexes featuring azahelicene (dibenzo[*c,g*]carbazole and benzo[*c*]carbazole) and enantio-pure chiral *N*-heterocyclic carbene (NHC) ligands with a complementary tailored shape. Crystallization of these azahelicene Au(I) complexes not only suppresses the dynamic chirality of the dibenzocarbazole species, but also stabilizes their homochirality through the intermolecular conjunction between the chiral NHC and dibenzocarbazole ligands. In the Au(I) benzocarbazole complexes, the intermolecular conjunction and chirality transfer in the crystals induces chirality in the initially achiral benzocarbazole ligand. Furthermore, the crystallization of the studied complexes activates their circularly polarized luminescence (CPL) properties, which were suppressed in solution. Importantly, chirality transfer to significant CPL enhancement; the complexes that feature chirality transfer within the crystal structure exhibit luminescence dissymmetry factors 5 to 10 times higher than those of the complexes without chirality transfer.

INTRODUCTION

Angularly annulated polyaromatic compounds such as helicenes,[1] twistacenes,[2] and related twisted polyaromatic systems[3, 4] are currently gaining significant attention due to their ability to exhibit helical chirality (Figure 1a). This unique feature makes them promising for applications in chiroptical devices,[5, 6] asymmetric catalysis,[7-9] organic electronics,[10] molecular machines,[11, 12] and medicinal chemistry.[13, 14] Since the helical chirality in these systems originates from strain-induced twist,[3] low-strain annulated π-systems with low-lying conformational flip barriers can exhibit dynamic chirality, allowing interconversion between enantiomers (Figure 1b).[15-17] Although this dynamic chirality can sometimes be exploited to obtain chirality-switchable properties,[18] as well as easy access to different conformers of a polyaromatic species,[19] it often merely results in racemization, which negates most of the valuable properties derived from helical homochirality. Therefore, stabilizing the homochirality of these systems is crucial to preserve their unique properties.

The most common approach to suppress dynamic chirality in polyaromatic species is kinetic stabilization of their conformation by introducing bulky substituents in the polyaromatic scaffold, interlocking the system and dramatically increasing the conformational flip barrier.[20, 21] However, enantioselective reactions during synthesis or subsequent chiral resolution of the formed enantiomeric mixture during isolation is required,[22] which can be laborious and challenging.

Another approach involves chirality transfer via the introduction of a chiral auxiliary group to a twisted and flexible polyaromatic system (Figure 1c). As demonstrated on perylene-diimide-based twistacene species, intramolecular chirality transfer can be achieved using chiral auxiliary groups that induce strain in the polyaromatic ribbon (Figure 1d),[23] steric repulsion (Figure 1e),[24, 25] or attractive through-space interactions between molecule fragments (Figure 1f).[26] Additionally, intermolecular chirality transfer from a molecule with persistent chirality to a conformationally flexible perylene-diimide-based cyclophane species resulted in the stabilization of one of the conformational enantiomers of the cyclophane through host–guest interactions in solution (Figure 1g).[27] Conversely, the binding of flexible helicene guests exhibiting dynamic chirality by homochiral hosts resulted in enantiomerization of enantiomerically pure guests[28] or deracemization of racemic guest mixtures[29] due to a reduced enantiomerization barrier (Figure 1h).

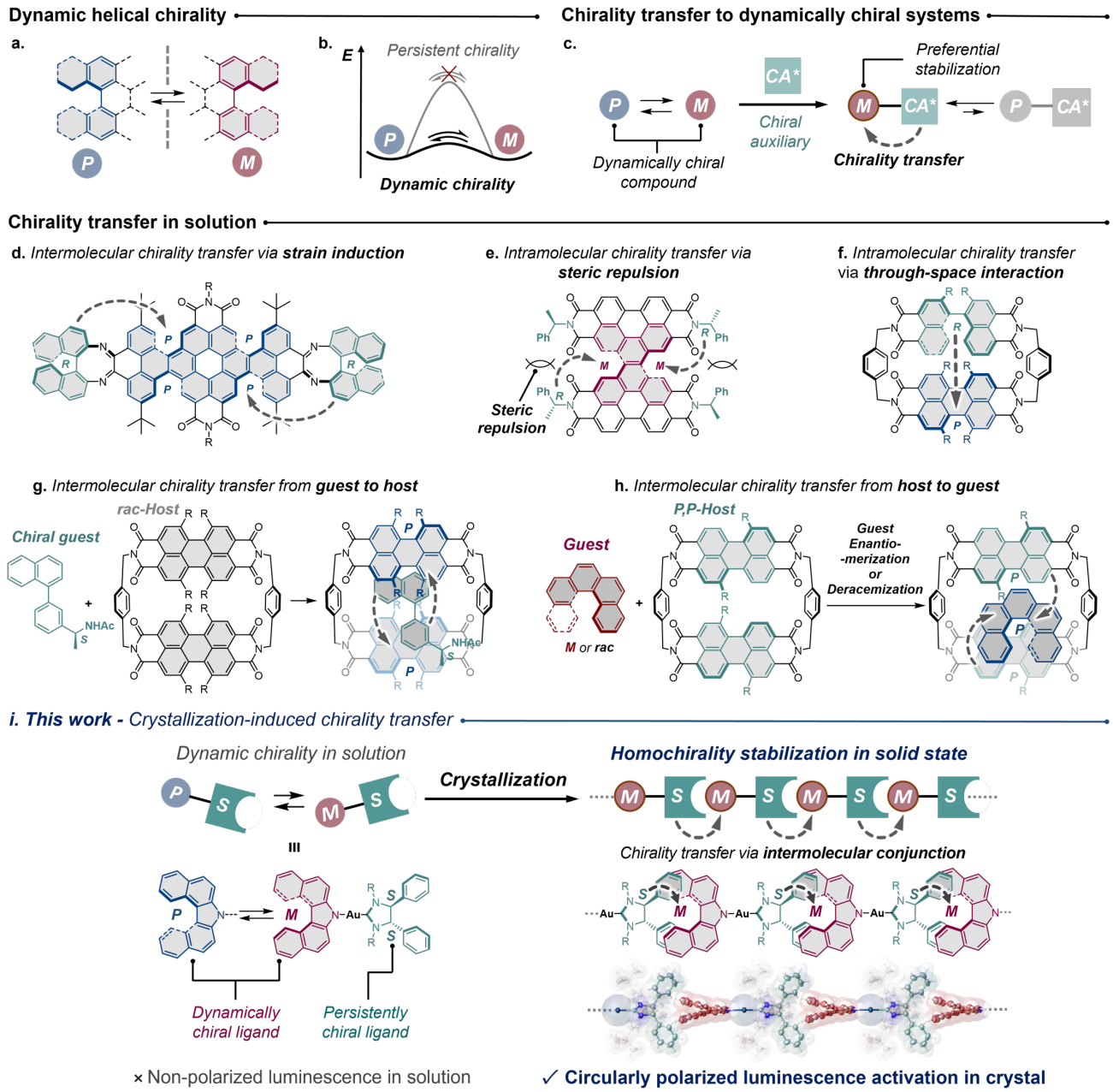

Figure 1. Dynamic helical chirality in polyaromatic systems and its stabilization though chirality transfer in solution and the solid state.

Remarkably, the chirality transfer can also influence the properties of dynamic twistacene systems, such as solvent- and redox-dependent electronic circular dichroism[24, 25] and circularly polarized luminescence.[26] This demonstrates the promise of chirality transfer to flexible polyaromatic systems as a strategy for constructing new systems with chirality-induced functionality.

Because the abovementioned examples of dynamic chirality control via chirality transfer operate in solution, in some cases, the effect is limited to preferential thermodynamic stabilization of one of the conformers without complete suppression of dynamic chirality. That is, interconversion between the different forms of the studied species may still occur in solution. In this work, we introduce a new approach for dynamic chirality stabilization in azahelicene species via crystallization-induced intermolecular chirality transfer in Au(I) complexes featuring a rigid enantio-pure *N*-heterocyclic carbene (NHC) ligand with persistent chirality and a conformationally flexible azahelicene ligand, namely, dibenzo[*c,g*]carbazole or benzo[*c*]carbazole. In solution, the NHC Au(I) dibenzocarbazole complexes exhibit dynamic chirality with very rapid exchange between the *P*- and *M*-conformers (Figure 1i). However, when an NHC ligand with a shape tailored for complementary interactions is used, the crystallization of these complexes can not only suppress the dynamic chirality of the dibenzocarbazole moiety, but also induce and stabilize homochirality through intermolecular chirality transfer by the intermolecular conjunction between the chiral NHC and dibenzocarbazole ligands in the crystal. In the case of the Au(I) benzocarbazole complexes, the presence of a similar conjunction between the molecules in the crystals induces chirality in the initially achiral benzocarbazole ligand.

Moreover, the crystallization of these complexes activates their circularly polarized luminescence (CPL), which was suppressed in solution due to dynamic chirality. Notably, the complexes exhibiting intermolecular chirality transfer in their crystals display a dramatic 5–10-fold enhancement in their luminescence dissymmetry factor values compared to the structures without direct chirality transfer. We believe that our approach to engineering intermolecular chirality transfer will be useful for the development of new types of solid-state chiral materials.

RESULTS AND DISCUSSION

Synthesis and Characterization of NHC Au(I) Azahelicene Complexes in Solution. To explore the potential for ligand-to-ligand chirality transfer in NHC Au(I) azahelicene complexes, we investigated a set of NHC and carbazole ligands (Scheme 1). 1,3-Bis(3,5-di-*tert*-butylbenzyl)-imidazolinium scaffolds with various substituents at the 4- and 5-positions of the imidazolinium backbone were utilized to study the capability NHC ligand of chirality transfer: the unsubstituted achiral NHC (**1**) (as a reference structure), the cyclohexyl-substituted NHC enantiomer pair [**2**-(*S,S*) and **2**-(*R,R*)], and the diphenyl-substituted enantiomer pair [**3**-(*S,S*) and **3**-(*R,R*)]. The azahelicene ligands were benzo[*c*]carbazole (**BCz**), which served as a reference structure with no inherent chirality, and dibenzo[*c,g*]carbazole (**DBCz**), which is capable of displaying dynamic chirality in solution. In the latter case, the presence of the 5-membered pyrrole core should result in very rapid *P/M*-exchange dynamics due its relatively low strain compared to similar [5]helicene species.[15, 30] The target NHC Au(I) azahelicene complexes [**1**–**3**-(*S,S*)- and **1**–**3**-(*R,R*)-DBCz; **3**-(*S,S*)- and **3**-(*R,R*)-BCz] were obtained in 84–96% yields by reacting the corresponding NHC Au(I) chloride complexes and DBCz or BCz in the presence of potassium *tert*-butoxide in THF solution at 45 °C. All complexes were characterized using ^{1}H and ^{13}C NMR spectroscopy, high-resolution mass-spectrometry (HRMS), C, H, N elemental analysis, single-crystal and powder X-ray diffraction (SCXRD and PXRD), circular dichroism (CD), photoluminescence, and circularly polarized luminescence (CPL) spectroscopy in solution and the solid state.

For all complexes, the solution-state ^{1}H and ^{13}C NMR spectra display only one set of signals, indicating that either only a single species is present, or the annulated carbazole ligands undergo *P*/*M*-exchange that is too rapid to be observed on the NMR timescale. Therefore, to investigate the potential dynamic chirality and intramolecular chirality transfer for the obtained complexes in solution, we conducted a theoretical investigation of the energy barriers for interconversion and the relative stability of the two possible *P*-/*M*-conformers of the **3**-(*S,S*)-DBCz complex, as well as of the structure of **3**-(*S,S*)-BCz in CH_2Cl_2 (using the PBE0-D3(BJ)/def2TZVP+MDF60/SMD(CH_2Cl_2) level of theory[31-37]). The optimization of **3**-(*S,S*)-BCz yields a structure featuring an overall flat BCz moiety; therefore, the BCz ligand should not possess any chirality and should exist in a single form in solution (Figure S1). In contrast, for the **3**-(*S,S*)-DBCz complexes, two structures featuring the *P*- and *M*-conformation of DBCz moiety could be present in solution with an energy difference (ΔG_{298}) of 0.5 kcal/mol and a DBCz conformation flip energy barrier ($\Delta G^{\ddagger}$) of ca. 3.5 kcal/mol (Table S2). The obtained energy values support the presence of a very fast exchange process between the *P*- and *M*-conformers.[15, 38] The small conformation flip barrier as well as small energy difference between the conformers imply the absence of intramolecular chirality transfer from the NHC to the DBCz ligands.

Crystal Structures and Chirality Transfer. Crystallization of the obtained complexes (for details, see Section S2.4) yielded crystalline samples with no solvent inclusion. The obtained single crystals were characterized by SCXRD at 293 K. The composition of the bulk crystalline samples was confirmed by PXRD at room temperature and elemental analysis. The crystal structures of all the complexes are presented in Figures 2 and 3, while the crystal data parameters are listed in Tables S3–S5 in the Supporting Information.

Scheme 1. Synthesis and Dynamic Chirality of NHC Au(I) Azahelicene Complexes in Solution

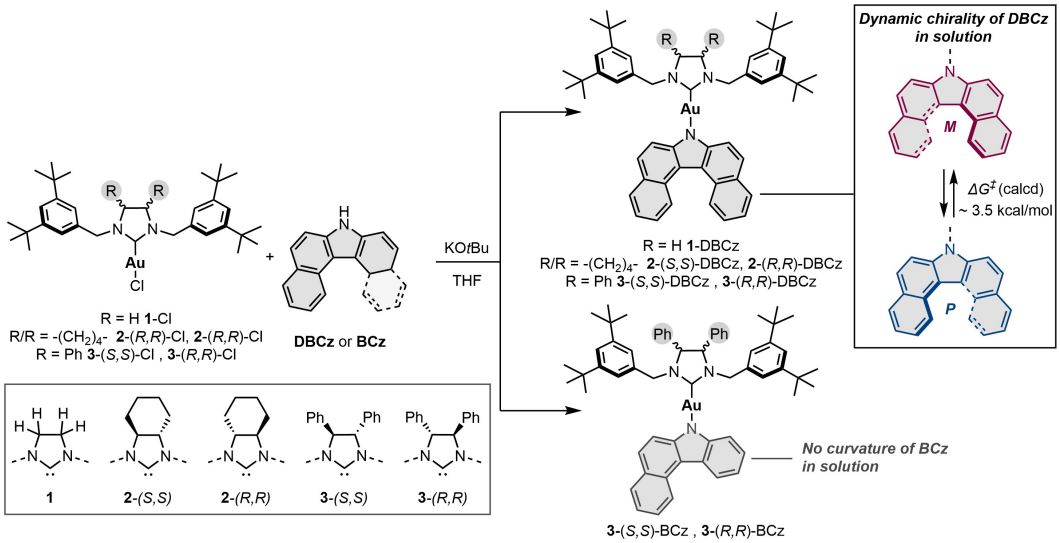

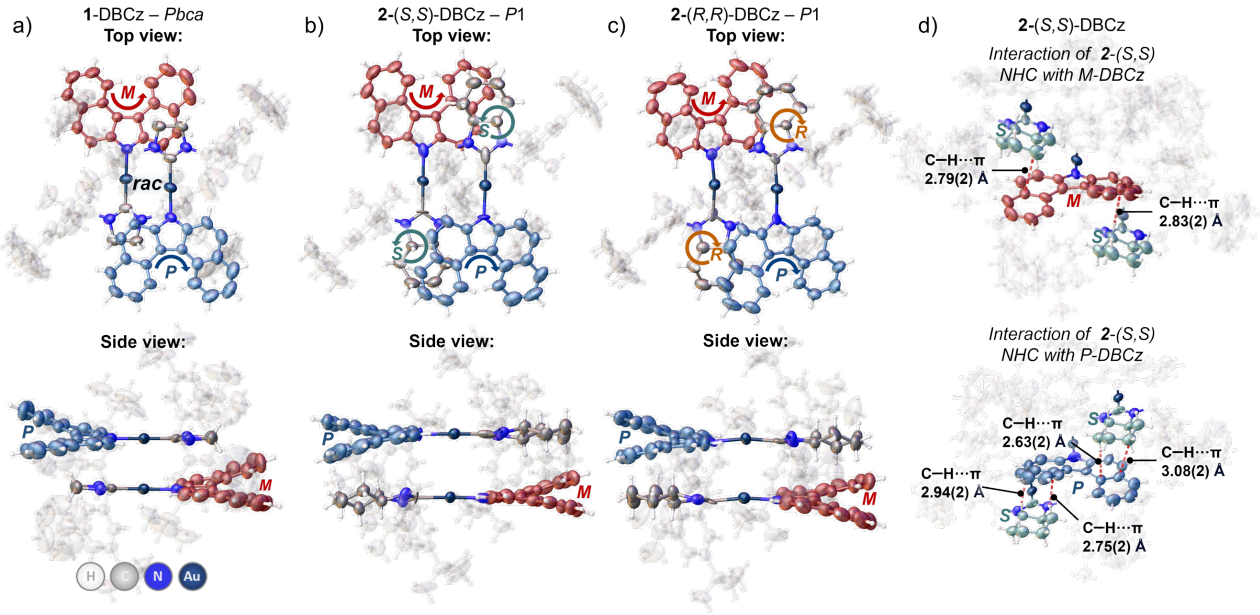

Figure 2. Crystal structures of **1**-DCBz (a), **2**-(*S,S*)-DBCz (b), and **2**-(*R,R)*-DBCz (c). The colors of the DBCz ligands indicate their configuration (blue: *P*; red: *M*), while those of the circular arrows indicate the configuration of the chiral center in the NHC ligand (*S*: cyan; *R*: orange). (d) C–H···π interactions (red dashed lines) between the **2**-(*S,S*)-NHC ligand and the *P*- or *M*-DBCz ligands in the structure of **2**-(*S,S)*-DBCz.

The crystal structure of **1**-DBCz with an achiral NHC ligand features the centrosymmetric *Pbca* space group. The asymmetric unit consists of only one molecule of the complex, while the unit cell contains four pairs of molecules, featuring both *P*- and *M*-curved DBCz moieties. Therefore, the crystal of **1**-DBCz can be considered a true racemate (Figure 2a).

The crystal structures of **2**-(*S,S*)- and **2**-(*R,R)*-DBCz display a similar packing pattern to that observed for **1**-DBCz (Figures S6–S7). Although the crystal structures of the **2**-(*S,S*)- and **2**-(*R,R*)-DBCz complexes feature a non-centrosymmetric *P*1 space group, they contain both *P*- and *M*-curved DBCz ligands in a 1:1 ratio, forming a diastereomeric mixture in the crystal (Figure 2b,c). Thus, the introduction of the chiral *S,S*- or *R,R*-cyclohexyl moiety in the NHC backbone does not cause direct chirality transfer from the NHC to the DBCz ligand in either solution or the solid state. However, it should be mentioned that the *P*- and *M*-curved DBCz ligands of **2**-(*S,S*)- and **2**-(*R,R*)-DBCz have different packing environments and exhibit different non-covalent interactions with the NHC ligand. For example, for **2**-(*S,S*)-DBCz, the *M*-curved DBCz ligand is involved in only one short C–H···π contact with each of the neighboring *S,S*-cyclohexyl fragments in the NHC ligands, while the *P*-DBCz forms two C–H···π interactions with each NHC fragment (Figure 2d). The opposite pattern was observed for **2**-(*R,R*)-DBCz.

Unlike the previous examples, the **3**-(*S,S*)- and **3**-(*R,R*)-DBCz complexes, which contain a chiral diphenyl moiety in the NHC backbone, crystallize in an enantiomorphic (chiral) space group pair: $P4_12_12$ and $P4_32_12$, respectively. Each complex features only one type of curved DBCz ligand, i.e., the *M*-conformation in **3**-(*S,S*)-DBCz (Figure 3a) and the *P*- one in **3**-(*R,R*)-DBCz (Figure 3b). The fixation of the homochiral conformation of the DBCz ligand suggests that the "hinge"-shaped chiral **3**-(*S,S*)- and **3**-(*R,R*)-NHC ligands are capable of transferring chirality to the DBCz ligand. In the latter case, the transfer occurs through an intermolecular head-to-tail conjunction between the NHC diphenyl moiety and the DBCz ligand assisted by intermolecular C–H···π interactions (Figure 3a,b and Figure S2). Additionally, in both crystal structures, the molecules of the complex form a helical supramolecular arrangement defined by the presence of a 4-fold screw axis in the unit cell: an *M*-helical packing for **3**-(*S,S*)-DBCz and a *P*-one for **3**-(*R,R*)-DBCz (Figure S8).

Surprisingly, the complexes **3**-(*S,S*)- and **3**-(*R,R*)-BCz, which featured achiral benzo[*c*]carbazole (BCz), resulted in crystal structures almost identical to those of the **3**-(*S,S*)- and **3**-(*R,R*)-DBCz pair: both the ***3***-(*S,S*)-BCz and **3**-(*R,R*)-BCz crystal structures also have the $P4_12_12$ and $P4_32_12$ chiral space groups, as well as nearly the same unit cell parameters as **3**-(*S,S*)- and **3**-(*R,R*)-DBCz (Tables S4–S5). The observed similarity in the crystal packing of the **3**-(*S,S*)-/**3**-(*R,R*)-DBCz and **3**-(*S,S*)-/**3**-(*R,R*)-BCz crystals is possibly due to the disorder of the BCz moiety in two positions in the crystals (Figure S9), which "mimics" the shape of the DBCz ligand in the structures of **3**-(*S,S*)- and **3**-(*R,R*)-DBCz. Furthermore, the similar crystal packing effects and the presence of intermolecular head-to-tail conjunction between the NHC and BCz ligands also cause the BCz moiety, which is initially achiral and planar in solution (according to DFT calculations), to adopt a chiral curvature in the solid state due to chirality transfer from the NHC ligand (Figure 3c,d). As a result, the obtained structures can be described as **3**-(*S,S*)-BCz-(*M*) and **3**-(*R,R*)-BCz-(*P*). The key structural difference between the DBCz- and BCz-derived structures is the degree of curvature of the DBCz- and BCz moieties. The torsion angles (Table S6) between the aryl planes demonstrate that the DBCz ligand in **3**-(*S,S*)- and **3**-(*R,R*)-DBCz is almost twice as curved as the BCz in **3**-(*S,S*)- and **3**-(*R,R*)-BCz.

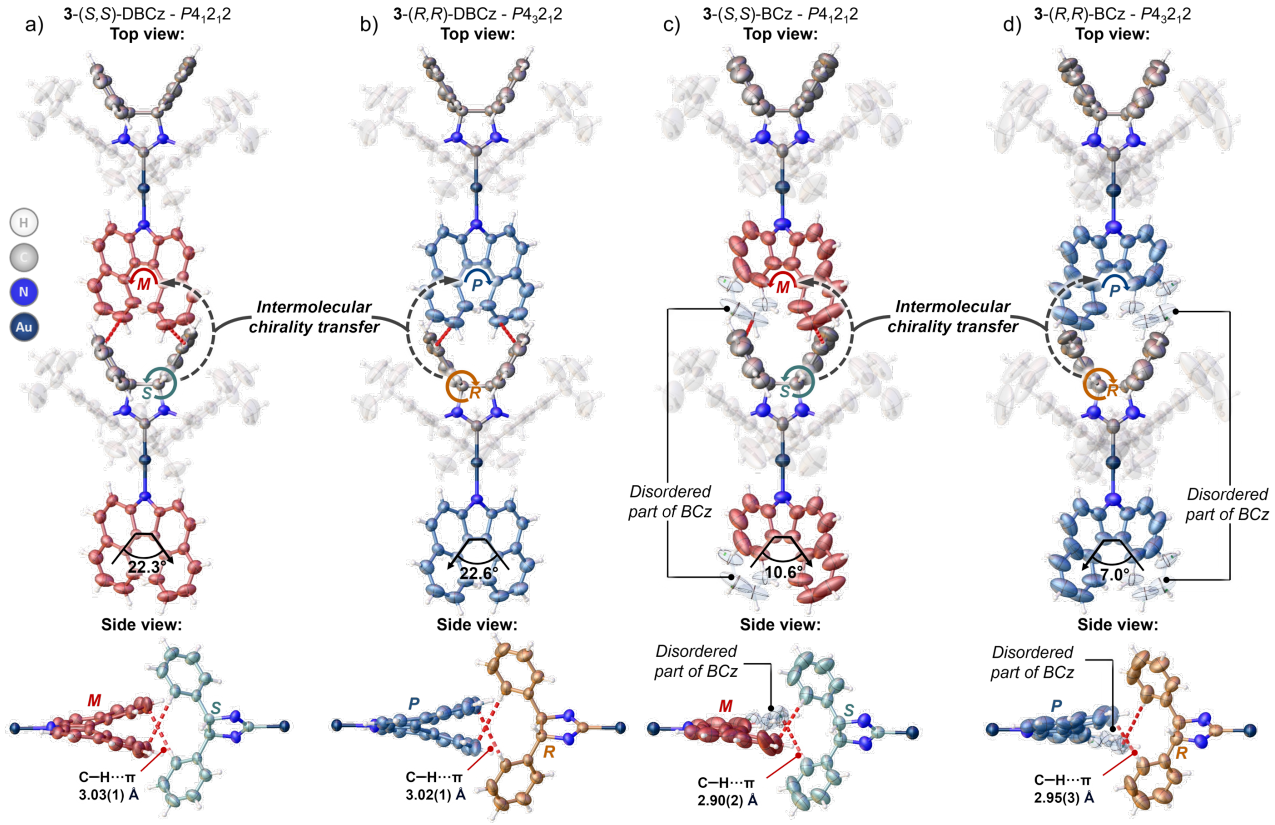

Figure 3. Crystal structures of **3**-(*S,S*)-DBCz (a), **3**-(*R,R*)-DBCz (b), **3**-(*S,S*)-BCz (c), and **3**-(*R,R*)-BCz (d). In the side views, the fragments not participating in chirality transfer have been omitted for clarity. The colors of the DBCz/BCz ligands indicate the configuration (blue: *P*; red: *M*), while those of the circular arrows indicate the configuration of the chiral center in the NHC ligand (*S*: cyan; *R*: orange). C–H···π interactions are indicated by the red dashed lines. In the case of **3**-(*S,S*)-BCz (c) and **3**-(*R,R*)-BCz, transparent ellipsoids depict one of the disordered parts of the benzo moiety in BCz.

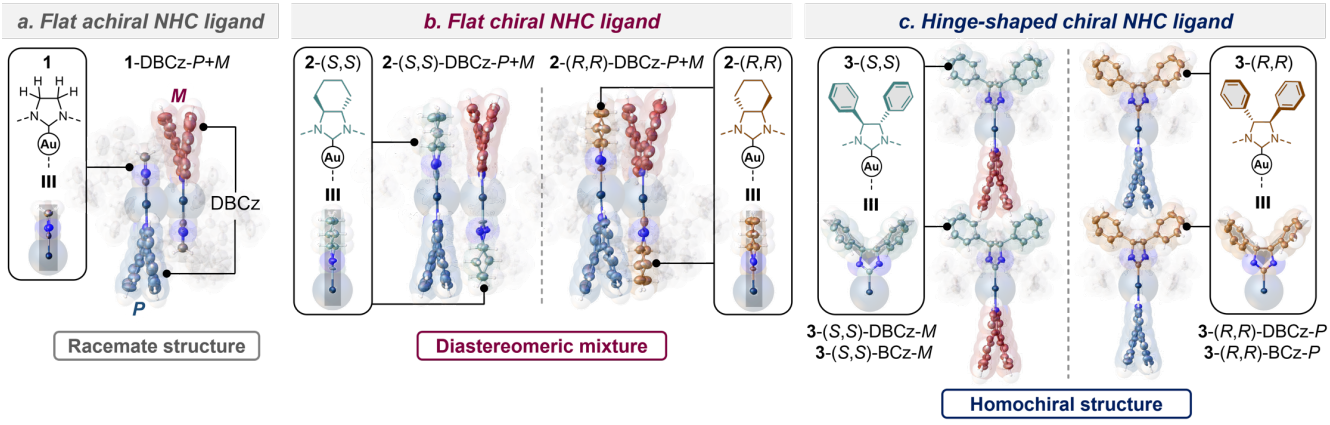

Figure 4. Relationship between the shape of the NHC ligand and the chirality in the crystals of the NHC Au(I) azahelicene complexes.

From the obtained structural data, we can conclude that the structure and shape of the NHC ligand play a crucial role in the chirality transfer to azahelicene ligands in the solid state. The obtained structures can be categorized into three cases (Figure 4):

a) The **1**-DBCz complex, in which an achiral NHC ligand forms racemate crystals containing both *P*- and *M*-DBCz moieties.

b) The **2**-(*S,S*)- and **2**-(*R,R*)-DBCz complexes, which have flat chiral NHC ligands that are not capable of chirality transfer, result in a diastereomeric mixture with both *P*- and *M*-DBCz moieties in the crystals.

c) The **3**-(*S,S*)- and **3**-(*R,R*)-DBCz/BCz complexes, featuring "hinge"-shaped chiral NHC ligands capable of direct chirality transfer, form homochiral crystal structures with either *P*- or *M*-DBCz/BCz moieties.

This indicates that the mere presence of an additional chiral moiety in the molecule is not sufficient to induce direct chirality transfer and the exclusive stabilization of either the *M*- or *P*-DBCz conformation. In the case of the **2**-(*S,S*)- and **2**-(*R,R*)-DBCz crystals, the flat shape of the cyclohexyl moiety in the

NHC ligand and its inability to form a conjunction with the DBCz ligand result in the coexistence of both *M*- and *P*-DBCz moieties in the crystal, along with a crystal packing similar to the racemate crystal of **1**-DBCz. On the contrary, the bulkier and hinge-shaped diphenyl moiety in **3**-(*S,S*)- and **3**-(*R,R*)-DBCz/BCz is capable of forming a "complimentary pair" with the DBCz/BCz ligands. This leads not only to the stabilization of one form of the DBCz ligand through direct chirality transfer, but also to the induction of chirality in the initially achiral BCz ligand.

Chiroptical and Emission Properties of NHC Au(I) Azahelicene Complexes. The coordination of DBCz and BCz ligands to the Au(I) center leads to a ca. 30 nm red-shift of their absorption in dichloromethane (DCM) solution, while the overall absorption profile remains mostly unchanged (Figure 5a for **1**-DBCz and Figures S18–19 for the other complexes). Additionally, the absorption within 250–280 nm range should also correspond to the NHC Au(I) fragment, similarly to the NHC Au(I) chloride precursor complexes. In the solid state, all complexes exhibit a slightly red-shifted absorption profile that is nearly identical in shape to that in DCM solution (Figure 5a and Figure S19).

Based on an analysis of the experimental spectra and the conducted TD-DFT calculations (Figure 5b and Figures S3–S5), the absorption spectrum of the obtained NHC Au(I) azahelicene complexes can be divided into three regions. From the higher wavelengths down to 350 nm, the absorption is mainly attributed to states involving only DBCz/BCz intra-ligand charge transfer (ILCT) with a slight admixture of Au(I)-to-DBCz/BCz metal-to-ligand charge transfer (MLCT). Below 350 nm, there is a noticeable contribution from ligand-to-ligand (LLCT) charge transfer involving both the NHC and DBCz/BCz moieties. Lastly, from 300 nm to 250 nm, in addition to the absorption from the DBCz ligand, there are ILCT/MLCT bands involving the NHC ligand.

As expected, **1**-DBCz does not exhibit any circular dichroism (CD) signal in DCM solution due to the absence of a chiral moiety in the NHC ligand and the fast *P/M*-exchange of the DBCz ligand (Figure S20). The absence of a CD response was also observed for the crystalline sample of **1**-DBCz due to the presence of two equivalent *P*- and *M*-DBCz moieties in the racemate crystal structure.

In contrast, upon introducing the chiral cyclohexyl moiety in the NHC backbone, the **2**-(*S,S*)- and **2**-(*R,R*)-DBCz complexes exhibit a distinct mirrored CD profiles in DCM solution (Figure 6a, blue lines). Almost no CD signal was observed in the range of 350–400 nm corresponding to DBCz absorption. However, in the lower wavelength region, two CD areas with opposite Cotton effects are observed, with CD maxima at 330 nm and 256 nm and absorption dissymmetry factor ($|g_{abs}|$) values of 1.4–1.8 × 10^{-4} and 4.5–4.7 × 10^{-4}, respectively. These Cotton effect maxima can be attributed to the absorption of the NHC Au(I) fragment, and the sign of the Cotton effect in this region is the same as that of the precursor **2**-(*S,S*)- and **2**-(*R,R*)-Cl complexes (Figure S20). In the crystalline state, the **2**-(*S,S*)- and **2**-(*R,R*)-DBCz complexes exhibit an inversion of the CD signal in the region from 280 nm to 425 nm compared to that in solution (Figure 6a, red lines). Additionally, a weak CD signal emerges at ca. 387 nm ($|g_{abs}|$ = 0.3–0.6 × 10^{-3}), and the CD signal at 327 nm is amplified, with $|g_{abs}|$ values of 1.2–1.3 × 10^{-3}. These regions correspond to the DBCz ligand, and the transition from the solution to crystalline state leads to an almost one order of magnitude increase in their $|g_{abs}|$ values. This could be caused by the elimination of the *P*-/*M*-exchange of the DBCz ligand and the confirmational fixation in the solid state. At the same time, in the absence of direct chirality transfer in the crystal, the appearance and increase of the CD response in these regions can be attributed to the presence of asymmetry in the packing environment of the *P*- and *M*-DBCz ligands observed in the crystals.

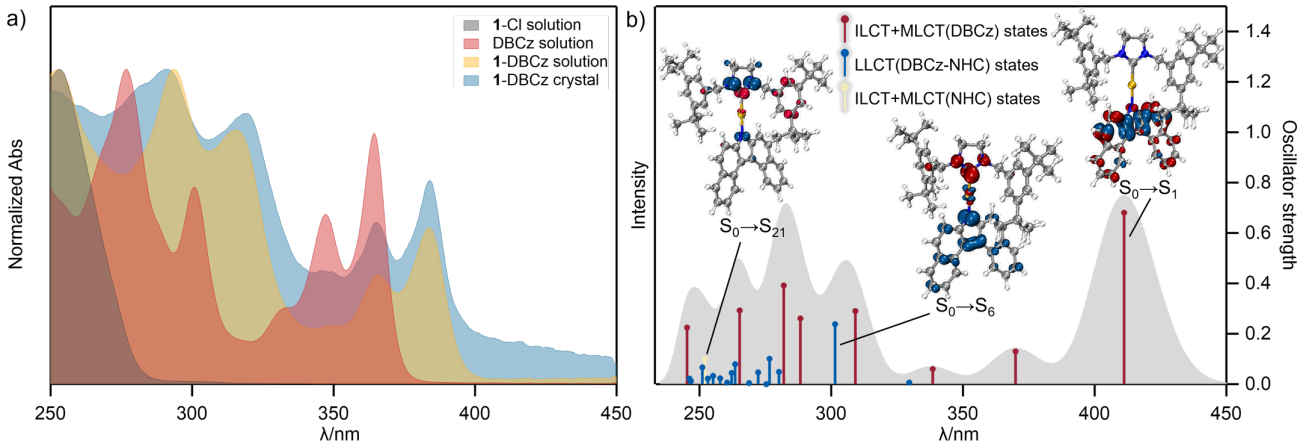

Figure 5. a) Absorption spectra of **1**-Cl (gray, 1.2 × 10^{-4} M), DBCz (red, 2 × 10^{-5} M), and **1**-DBCz (yellow, 2 × 10^{-5} M) in DCM solution, and of **1**-DBCz in the solid state (blue, 2% *w/w* in paraffin oil). b) Calculated TD-DFT absorption spectrum and oscillator strengths of **1**-DBCz-(*M*) with the hole–electron distribution maps[39] (isovalue 0.003) for the selected transitions: hole distribution is indicated in blue and electron distribution in red.

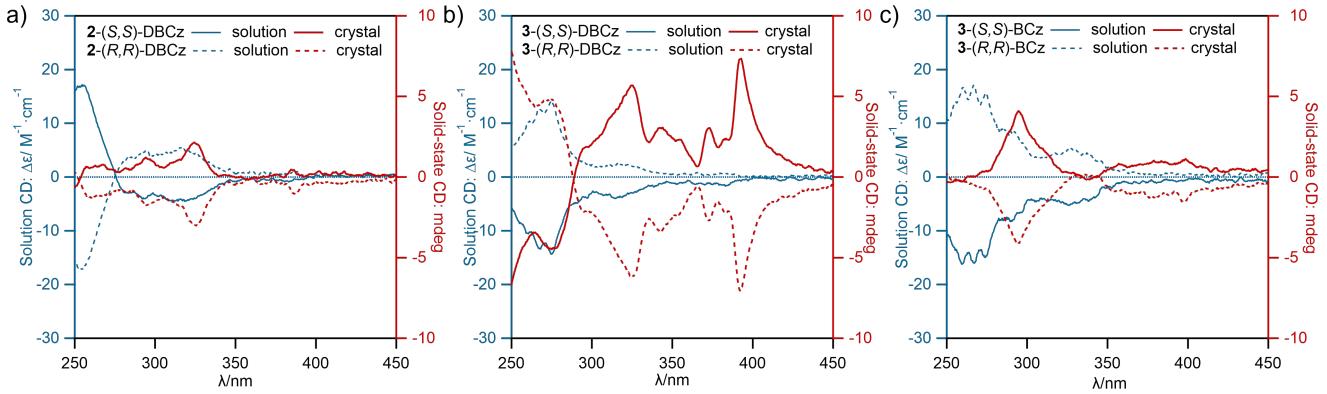

Figure 6. CD spectra of **2**-(*S,S*)- and **2**-(*R,R*)-DBCz (a), **3**-(*S,S*)- and **3**-(*R,R*)-DBCz (b), **3**-(*S,S*)- and **3**-(*R,R*)-BCz (c) complexes in DCM solution (blue lines, left CD axis, 2×10^{-5} M) and solid state (red lines, right CD axis, 2% *w/w* in paraffin oil). The CD values for the solution and solid state cannot be compared directly due to the different sample measurement methods (see Section S6 for details).

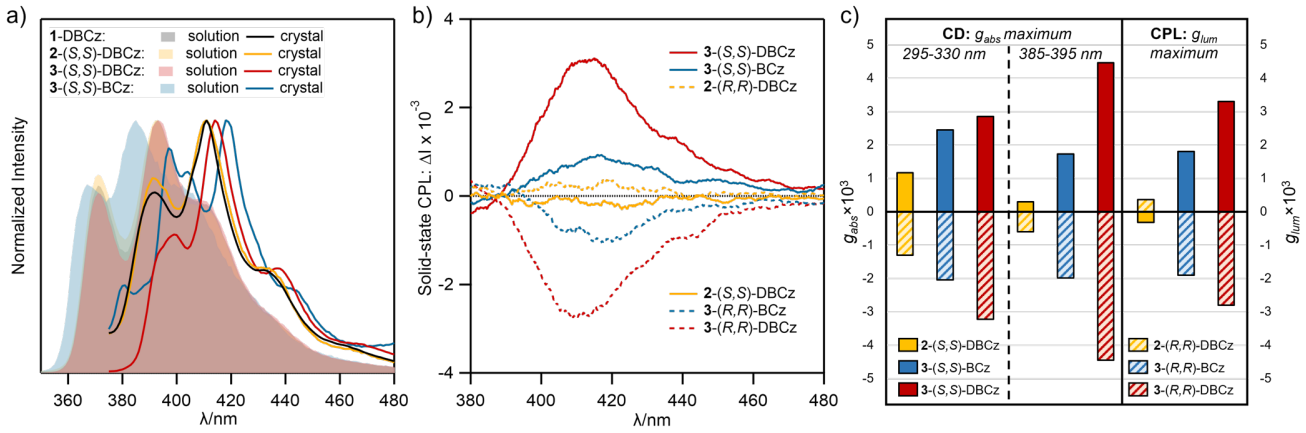

Figure 7. a) Normalized emission spectra of the **1**-DBCz, **2**-(*S,S*)-DBCz, **3**-(*S,S*)-DBCz, **3**-(*S,S*)-BCz complexes in DCM solution (filled area, 2×10^{-5} M) and solid state (lines, 10% *w/w* in paraffin oil). b) CPL spectra of NHC Au(I) azahelicene complexes in the solid state (10% *w/w* in paraffin oil). c) Bar chart of absorption and luminescence dissymmetry factor maximum values (g_{abs} and g_{lum}) of NHC Au(I) azahelicene complexes in the solid state; the data is taken from Table S9.

While the complexes **3**-(*S,S*)- and **3**-(*R,R*)-DBCz and -BCz show similar CD response levels to **2**-(*S,S*)- and **2**-(*R,R*)-DBCz in DCM solution, more significant changes in the CD profiles were observed after crystallization. In DCM solution, all the **3**-(*S,S*)-/**3**-(*R,R*)-DBCz and -BCz complexes exhibit quite similar CD profiles with maxima at 275 nm ($|g_{abs}| = 5.6–5.8 \times 10^{-4}$) for **3**-(*S,S*)- and **3**-(*R,R*)-DBCz and 267 nm ($|g_{abs}| = 3.8–4.2 \times 10^{-4}$) for **3**-(*S,S*)- and **3**-(*R,R*)-BCz, while in the DBCz and BCz absorption regions, the CD response is noticeably weaker: the CD maxima were observed at 316 nm for **3**-(*S,S*)- and **3**-(*R,R*)-DBCz ($|g_{abs}| = 0.9–1.2 \times 10^{-4}$) and at 297 nm for **3**-(*S,S*)- and **3**-(*R,R*)-BCz ($|g_{abs}| = 2.0–2.1 \times 10^{-4}$) (Figures 6b,c, blue lines). Conversely, after crystallization, a strong increase in the CD signals in the DBCz and BCz absorption regions was observed. The complexes **3**-(*S,S*)- and **3**-(*R,R*)-DBCz display two main CD maxima at 324 nm and 392 nm with $|g_{abs}|$ values of 2.45–3.22×10^{-3} and 4.45–4.46×10^{-3}, respectively. In the case of **3**-(*S,S*)- and **3**-(*R,R*)-BCz, the maximum CD response was observed at 295 nm with a $|g_{abs}|$ value of 2.04–2.45×10^{-3} which also corresponds to its absorption maximum. Noteworthily, similarly to the **2**-(*S,S*)- and **2**-(*R,R*)-DBCz complexes, the crystallization of the **3**-(*S,S*)- and **3**-(*R,R*)-DBCz complexes, as well as the **3**-(*S,S*)- and **3**-(*R,R*)-BCz complexes, also leads to the inversion of the CD signal above 280 nm for **3**-(*S,S*)- and **3**-(*R,R*)-DBCz and above 255 nm for **3**-(*S,S*)- and **3**-(*R,R*)-BCz relative to their solution spectra. Based on the obtained CD data, it can be seen that the **3**-(*S,S*)-/**3**-(*R,R*)-complexes of -DBCz and -BCz, which feature direct chirality transfer from the NHC to the DBCz/BCz ligands, display a stronger CD response in the DBCz/BCz absorption regions than the **2**-(*S,S*)- and **2**-(*R,R*)-DBCz complexes in the solid state (Figure 6).

In DCM solution, all complexes with a DBCz ligand exhibit similar photoluminescence emission bands with maximum wavelengths in the range of 390–400 nm, indicating the minor effect of the substituent structure of the NHC ligand on the emission profile (Figure 7a). Notably, the emission of **3**-(*S,S*)- and **3**-(*R,R*)-BCz is blue-shifted compared to those of the other complexes, with an emission maximum at 386 nm. At the same time, in the crystalline state, a general emission red-shift of ca. 25–35 nm was observed for all complexes. In addition, the appearance of a weaker side band in the 450–600 nm region was observed for crystalline samples (Figure S24).

None of the obtained complexes display CPL properties in DCM solution, regardless of the excitation wavelength (Figure S26). This can be explained by the dynamic chirality of the DBCz moiety in solution and the absence of chirality transfer from the NHC ligand to the DBCz/BCz ligand. In contrast, in the solid state, all complexes except the racemic **1**-DBCz display a noticeable CPL response in the 390–470 nm region

(Figure 7b). The weakest CPL performance was observed for the complexes **2**-(*S,S*)- and **2**-(*R,R*)-DBCz, with luminescence dissymmetry factor $|g_{lum}|$ values of only 3.2–3.6 × 10^{-4} (Figure S27). Remarkably, these complexes display inverted CPL signals in comparison to their CD signals (the 320 nm band was used for excitation), as well as to the CPL signals of the other complexes. This may relate to the presence of both *P*- and *M*-DBCz ligands in their crystal structure. In contrast, the complexes **3**-(*S,S*)- and **3**-(*R,R*)-DBCz, which feature direct chirality transfer from the NHC to the DBCz ligand and only one type of DBCz ligand, display an almost 10-fold increase in their $|g_{lum}|$ values (2.8–3.3 × 10^{-3}) compared to **2**-(*S,S*)- and **2**-(*R,R*)-DBCz (Figures 7b and c). Additionally, the complexes **3**-(*S,S*)- and **3**-(*R,R*)-BCz, which have almost the same crystal structure as their DBCz-derived analogs, show inferior CPL with $|g_{lum}|$ values of 1.8–1.9 × 10^{-3}.

To summarize the obtained CD and CPL results, a consistent trend emerges across the obtained complexes. In solution, none of the complexes featuring chiral NHC ligands show any CPL signal, and they have a weak CD response in the DBCz/BCz absorption regions, mainly due to the flexibility of DBCz and the lack of chirality transfer. Conversely, in the solid state, a clear connection was observed between the crystal structure and both the CPL and CD response levels (Figure 7c). The crystals of **2**-(*S,S*)- and **2**-(*R,R*)-DBCz, which include both *P*- and *M*-DBCz moieties that are not involved in direct chirality transfer, demonstrate the lowest luminescence and absorption dissymmetry factor values in the series. The **3**-(*S,S*)- and **3**-(*R,R*)-DBCz/BCz complexes, which feature a "hinge"-shaped diphenyl moiety capable of chirality transfer, exhibit much better CPL performance and stronger CD responses. Despite the almost identical crystal packing of these DBCz- and BCz-derived complexes, their luminescence and absorption dissymmetry factors differ, which can be attributed to the difference in the structure and degree of curvature of the annulated carbazole ligands. This is similar to previously reported observations for other helicene systems, in which extending the helicene backbone increases the degree of curvature of the system and enhances both CPL and CD responses in solution.[40, 41] Likewise, in the case of the complexes **3**-(*S,S*)- and **3**-(*R,R*)-DBCz/BCz, the change from BCz to DBCz also leads to an increased degree of curvature in the carbazole ligand and enhanced CPL performance and CD response.

CONCLUSIONS

In this work, using a series of chiral *N*-heterocyclic carbene Au(I) dibenzo[*c,g*]carbazole and benzo[*c*]carbazole complexes, we have demonstrated how the shape of the chiral NHC ligand can enable chirality transfer in the crystal through intermolecular conjunction to stabilize the homochirality of the conformationally flexible azahelicene species. The presence of the "hinge"-shaped chiral diphenyl moiety in the NHC backbone of **3**-(*S,S*)- and **3**-(*R,R*)-DBCz/BCz resulted in the formation of intermolecular head-to-tail conjunction and chirality transfer between the chiral NHC and DBCz/BCz ligands, assisted by intermolecular C–H···π interactions. The complementary shape of the NHC backbone leads not only to selective fixation of one conformation of the dynamically chiral DBCz ligand in the crystal, but also to the induction of chirality in the initially achiral BCz ligand. Conversely, the smaller, flat cyclohexyl moiety in the NHC ligand of **2**-(*S,S*)- and **2**-(*R,R*)-DBCz does not induce chirality transfer in the crystals. Instead, it leads to the formation of diastereomeric mixture within the crystal and the coexistence of both *M*- and *P*-DBCz moieties. Moreover, crystallization activates the valuable CPL properties of the studied systems, which were suppressed in solution by the presence of dynamic chirality and absence of chirality transfer. In the crystalline state, a clear connection between the crystal structure and CPL properties was observed. Crystalline samples of the complexes **3**-(*S,S*)- and **3**-(*R,R*)-DBCz/BCz featuring direct chirality transfer and a single conformation of the DBCz/BCz ligand display ca. 5–10-fold enhancement in the g_{lum} value in comparison to **2**-(*S,S*)- and **2**-(*R,R*)-DBCz, which contain both *P*- and *M*-DBCz ligands in their crystal structure.

In the future, the present approach of intermolecular chirality transfer for the stabilization of homochirality in species with dynamic helical chirality could be expanded to other types of twisted organic and organometallic systems, and should be useful for the design of a new generation of crystalline and supramolecular chiral materials.

ASSOCIATED CONTENT

Supporting Information.

Supporting Information is available free of charge.
Experimental procedures, compound characterization, NMR, CD, CPL, PL spectra, crystallographic, and computational data (PDF)
Crystal information and structure factor files (ZIP)
Cartesian atomic coordinates used in the calculations (ZIP)

Accession Codes

CCDC 2321133-2321141 contain the supplementary crystallographic data for this paper. These data can be obtained free of charge via www.ccdc.cam.ac.uk/data_request/cif, or by emailing data_request@ccdc.cam.ac.uk, or by contacting The Cambridge Crystallographic Data Centre, 12 Union Road, Cambridge CB2 1EZ, UK; fax:+44 1223 336033.

AUTHOR INFORMATION

Corresponding Author

Mingoo Jin − *Institute for Chemical Reaction Design and Discovery (WPI-ICReDD), Hokkaido University, Sapporo, Hokkaido 060-8628, Japan;* orcid.org/0000-0001-6199-8802; Email: mingoo@icredd.hokudai.ac.jp

Hajime Ito − *Division of Applied Chemistry, Graduate School of Engineering, Hokkaido University, Sapporo, Hokkaido 060-8628, Japan; Institute for Chemical Reaction Design and Discovery (WPI-ICReDD), Hokkaido University, Sapporo, Hokkaido 001-0021, Japan;* orcid.org/0000-0003-3852-6721; Email: hajito@eng.hokudai.ac.jp

Authors

Pingyu Jiang − *Division of Applied Chemistry, Graduate School of Engineering, Hokkaido University, Sapporo, Hokkaido 060-8628, Japan;*

Alexander S. Mikherdov − *Institute for Chemical Reaction Design and Discovery (WPI-ICReDD), Hokkaido University, Sapporo, Hokkaido 001-0021, Japan;* orcid.org/0000-0002-6471-5158;

Author Contributions

‡P.J. and A.M. contributed equally. A.M. conceived and designed the study and prepared the initial manuscript draft. P.J. performed synthetic work, compounds characterization, photophysical studies, and analyzed the data. A.M. performed XRD analysis, photophysical studies, theoretical studies and analyzed the data. M.J. and H.I. supervised the work. All authors discussed the results, and the manuscript was written through contributions of all authors.

Notes

The authors declare no competing financial interest.

ACKNOWLEDGMENTS

This work was financially supported by the Japan Society for the Promotion of Science (JSPS) via KAKENHI grants JP17H06370, JP20H04666, JP21K14637, JP22K18333, and JP22H00318; by the JST via CREST grant JPMJCR19R1; and by the Institute for Chemical Reaction Design and Discovery (ICReDD), established by the World Premier International Research Initiative (WPI), MEXT, Japan. P.J. thanks the China Scholarship Council for the scholarship for PhD study (CSC 202108430010).

REFERENCES

(1) Shen, Y.; Chen, C.-F., Helicenes: Synthesis and Applications. *Chem. Rev.* **2012,** *112*, 1463–1535.
(2) Bedi, A.; Gidron, O., The Consequences of Twisting Nanocarbons: Lessons from Tethered Twisted Acenes. *Acc. Chem. Res.* **2019,** *52*, 2482–2490.
(3) Rickhaus, M.; Mayor, M.; Juríček, M., Strain-induced helical chirality in polyaromatic systems. *Chem. Soc. Rev.* **2016,** *45*, 1542–1556.
(4) Majewski, M. A.; Stępień, M., Bowls, Hoops, and Saddles: Synthetic Approaches to Curved Aromatic Molecules. *Angew. Chem., Int. Ed.* **2019,** *58*, 86–116.
(5) Mori, T., Chiroptical Properties of Symmetric Double, Triple, and Multiple Helicenes. *Chem. Rev.* **2021,** *121*, 2373–2412.
(6) Albano, G.; Pescitelli, G.; Di Bari, L., Chiroptical Properties in Thin Films of π-Conjugated Systems. *Chem. Rev.* **2020,** *120*, 10145–10243.
(7) Sakamoto, D.; Gay Sánchez, I.; Rybáček, J.; Vacek, J.; Bednárová, L.; Pazderková, M.; Pohl, R.; Císařová, I.; Stará, I. G.; Starý, I., Cycloiridated Helicenes as Chiral Catalysts in the Asymmetric Transfer Hydrogenation of Imines. *ACS Catal.* **2022,** *12*, 10793–10800.
(8) Yavari, K.; Aillard, P.; Zhang, Y.; Nuter, F.; Retailleau, P.; Voituriez, A.; Marinetti, A., Helicenes with Embedded Phosphole Units in Enantioselective Gold Catalysis. *Angew. Chem., Int. Ed.* **2014,** *53*, 861–865.
(9) Demmer, C. S.; Voituriez, A.; Marinetti, A., Catalytic uses of helicenes displaying phosphorus functions. *C. R. Chim.* **2017,** *20*, 860–879.
(10) Peurifoy, S. R.; Sisto, T. J.; Ng, F.; Steigerwald, M. L.; Chen, R.; Nuckolls, C., Dimensional Control in Contorted Aromatic Materials. *Chem. Rec.* **2019,** *19*, 1050–1061.
(11) Isla, H.; Crassous, J., Helicene-based chiroptical switches. *C. R. Chim.* **2016,** *19*, 39–49.
(12) Ravat, P.; Šolomek, T.; Juríček, M., Helicenes as Chiroptical Photoswitches. *ChemPhotoChem* **2019,** *3*, 180–186.
(13) Rushworth, J. L.; Thawani, A. R.; Fajardo-Ruiz, E.; Meiring, J. C. M.; Heise, C.; White, A. J. P.; Akhmanova, A.; Brandt, J. R.; Thorn-Seshold, O.; Fuchter, M. J., [5]-Helistatins: Tubulin-Binding Helicenes with Antimitotic Activity. *JACS Au* **2022,** *2*, 2561–2570.
(14) Summers, P. A.; Thomas, A. P.; Kench, T.; Vannier, J.-B.; Kuimova, M. K.; Vilar, R., Cationic helicenes as selective G4 DNA binders and optical probes for cellular imaging. *Chem. Sci.* **2021,** *12*, 14624–14634.
(15) Janke, R. H.; Haufe, G.; Würthwein, E.-U.; Borkent, J. H., Racemization Barriers of Helicenes: A Computational Study[1]. *J. Am. Chem. Soc.* **1996,** *118*, 6031–6035.
(16) Elm, J.; Lykkebo, J.; Sørensen, T. J.; Laursen, B. W.; Mikkelsen, K. V., Racemization Mechanisms and Electronic Circular Dichroism of [4]Heterohelicenium Dyes: A Theoretical Study. *J. Phys. Chem. A* **2011,** *115*, 12025–12033.
(17) Watanabe, M.; Suzuki, H.; Tanaka, Y.; Ishida, T.; Oshikawa, T.; Tori-i, A., One-Pot Synthesis of Helical Aromatics: Stereoselectivity, Stability against Racemization, and Assignment of Absolute Configuration Assisted by Experimental and Theoretical Circular Dichroism. *J. Org. Chem.* **2004,** *69*, 7794–7801.
(18) Chen, C.-T.; Tsai, C.-C.; Tsou, P.-K.; Huang, G.-T.; Yu, C.-H., Enantiodivergent Steglich rearrangement of *O*-carboxylazlactones catalyzed by a chirality switchable helicene containing a 4-aminopyridine unit. *Chem. Sci.* **2017,** *8*, 524–529.
(19) Weiss, C.; Sharapa, D. I.; Hirsch, A., Coronenohelicenes with Dynamic Chirality. *Chem. – Eur. J.* **2020,** *26*, 14100–14108.
(20) Mahlmeister, B.; Mahl, M.; Reichelt, H.; Shoyama, K.; Stolte, M.; Würthner, F., Helically Twisted Nanoribbons Based on Emissive Near-Infrared Responsive Quaterrylene Bisimides. *J. Am. Chem. Soc.* **2022,** *144*, 10507–10514.
(21) Gingras, M., One hundred years of helicene chemistry. Part 1: non-stereoselective syntheses of carbohelicenes. *Chem. Soc. Rev.* **2013,** *42*, 968–1006.
(22) Gingras, M.; Félix, G.; Peresutti, R., One hundred years of helicene chemistry. Part 2: stereoselective syntheses and chiral separations of carbohelicenes. *Chem. Soc. Rev.* **2013,** *42*, 1007–1050.
(23) Dubey, R. K.; Melle-Franco, M.; Mateo-Alonso, A., Inducing Single-Handed Helicity in a Twisted Molecular Nanoribbon. *J. Am. Chem. Soc.* **2022,** *144*, 2765–2774.
(24) Bao, S. T.; Jiang, H.; Schaack, C.; Louie, S.; Steigerwald, M. L.; Nuckolls, C.; Jin, Z., Remote Control of Dynamic Twistacene Chirality. *J. Am. Chem. Soc.* **2022,** *144*, 18772–18777.
(25) Bao, S. T.; Louie, S.; Jiang, H.; Jiang, Q.; Sun, S.; Steigerwald, M. L.; Nuckolls, C.; Jin, Z., Near-Infrared, Organic Chiroptic Switch with High Dissymmetry Factors. *J. Am. Chem. Soc.* **2023**. DOI: 10.1021/jacs.3c10578
(26) Ouyang, G.; Rühe, J.; Zhang, Y.; Lin, M.-J.; Liu, M.; Würthner, F., Intramolecular Energy and Solvent-Dependent Chirality Transfer within a BINOL-Perylene Hetero-Cyclophane. *Angew. Chem., Int. Ed.* **2022,** *61*, e202206706.
(27) Sapotta, M.; Spenst, P.; Saha-Möller, C. R.; Würthner, F., Guest-mediated chirality transfer in the host–guest complexes of an atropisomeric perylene bisimide cyclophane host. *Org. Chem. Front.* **2019,** *6*, 892–899.
(28) Weh, M.; Kroeger, A. A.; Shoyama, K.; Grüne, M.; Karton, A.; Würthner, F., π–π Catalysis Made Asymmetric—Enantiomerization Catalysis Mediated by the Chiral π-System of a Perylene Bisimide Cyclophane. *Angew. Chem., Int. Ed.* **2023,** *62*, e202301301.
(29) Weh, M.; Rühe, J.; Herbert, B.; Krause, A.-M.; Würthner, F., Deracemization of Carbohelicenes by a Chiral Perylene Bisimide Cyclophane Template Catalyst. *Angew. Chem., Int. Ed.* **2021,** *60*, 15323–15327.
(30) Caronna, T.; Mele, A.; Famulari, A.; Mendola, D.; Fontana, F.; Juza, M.; Kamuf, M.; Zawatzky, K.; Trapp, O., A Combined Experimental and Theoretical Study on the Stereodynamics of Monoaza[5]helicenes: Solvent-Induced Increase of the Enantiomerization Barrier in 1-Aza-[5]helicene. *Chem. – Eur. J.* **2015,** *21*, 13919–13924.
(31) Adamo, C.; Barone, V., Toward reliable density functional methods without adjustable parameters: The PBE0 model. *J. Chem. Phys.* **1999,** *110*, 6158–6170.
(32) Grimme, S.; Antony, J.; Ehrlich, S.; Krieg, H., A consistent and accurate *ab initio* parametrization of density functional dispersion correction (DFT-D) for the 94 elements H–Pu. *J. Chem. Phys.* **2010,** *132*, 154104.
(33) Grimme, S.; Ehrlich, S.; Goerigk, L., Effect of the damping function in dispersion corrected density functional theory. *J. Comput. Chem.* **2011,** *32*, 1456–1465.
(34) Figgen, D.; Rauhut, G.; Dolg, M.; Stoll, H., Energy-consistent pseudopotentials for group 11 and 12 atoms: adjustment to multi-configuration Dirac–Hartree–Fock data. *Chem. Phys.* **2005,** *311*, 227–244.
(35) Weigend, F.; Ahlrichs, R., Balanced basis sets of split valence, triple zeta valence and quadruple zeta valence quality for H to Rn: Design and assessment of accuracy. *Phys. Chem. Chem. Phys.* **2005,** *7*, 3297–3305.

(36) Weigend, F., Accurate Coulomb-fitting basis sets for H to Rn. *Phys. Chem. Chem. Phys.* **2006,** *8*, 1057–1065.
(37) Marenich, A. V.; Cramer, C. J.; Truhlar, D. G., Universal Solvation Model Based on Solute Electron Density and on a Continuum Model of the Solvent Defined by the Bulk Dielectric Constant and Atomic Surface Tensions. *J. Phys. Chem. B* **2009,** *113*, 6378–6396.
(38) Heeb, J.-P.; Clayden, J.; Smith, M. D.; Armstrong, R. J., Interrogating the configurational stability of atropisomers. *Nat. Protoc.* **2023**, *18*, 2745-2771.
(39) Liu, Z.; Lu, T.; Chen, Q., An sp-hybridized all-carboatomic ring, cyclo[18]carbon: Electronic structure, electronic spectrum, and optical nonlinearity. *Carbon* **2020,** *165*, 461–467.
(40) Qiu, Z.; Ju, C.-W.; Frédéric, L.; Hu, Y.; Schollmeyer, D.; Pieters, G.; Müllen, K.; Narita, A., Amplification of Dissymmetry Factors in π-Extended [7]- and [9]Helicenes. *J. Am. Chem. Soc.* **2021,** *143*, 4661–4667.
(41) Tian, X.; Shoyama, K.; Mahlmeister, B.; Brust, F.; Stolte, M.; Würthner, F., Naphthalimide-Annulated [n]Helicenes: Red Circularly Polarized Light Emitters. *J. Am. Chem. Soc.* **2023,** *145*, 9886–9894.